A Chandra X-Ray study of the dense globular cluster Terzan 5

DRAFT VERSION NOVEMBER 1, 2018
Preprint typeset using LaTeX style emulateapj v. 11/12/01

A *Chandra* X-RAY STUDY OF THE DENSE GLOBULAR CLUSTER TERZAN 5

C. O. HEINKE, P. D. EDMONDS, J. E. GRINDLAY, D. A. LLOYD
Harvard College Observatory, 60 Garden Street, Cambridge, MA 02138;
cheinke@cfa.harvard.edu, pedmonds@cfa.harvard.edu, josh@cfa.harvard.edu, dlloyd@cfa.harvard.edu
AND

H. N. COHN AND P. M. LUGGER
Department of Astronomy, Indiana University, Swain West 319, Bloomington, IN 47405; cohn@indiana.edu,
lugger@indiana.edu
Draft version November 1, 2018

ABSTRACT

We report a *Chandra* ACIS-I observation of the dense globular cluster Terzan 5. The previously known transient low-mass x-ray binary (LMXB) EXO 1745-248 in the cluster entered a rare high state during our August 2000 observation, complicating the analysis. Nevertheless nine additional sources clearly associated with the cluster are also detected, ranging from $L_X(0.5-2.5\mathrm{keV}) = 5.6\times10^{32}$ down to 8.6×10^{31} ergs s^{-1}. Their X-ray colors and luminosities, and spectral fitting, indicate that five of them are probably cataclysmic variables, and four are likely quiescent LMXBs containing neutron stars. We estimate the total number of sources between $L_X(0.5-2.5\mathrm{keV}) = 10^{32}$ and 10^{33} ergs s^{-1} as $11.4^{+4.7}_{-1.8}$ by the use of artificial point source tests, and note that the numbers of X-ray sources are similar to those detected in NGC 6440. The improved X-ray position allowed us to identify a plausible infrared counterpart to EXO 1745-248 on our 1998 *Hubble Space Telescope* NICMOS images. This blue star (F110W=18.48, F187W=17.30) lies within 0.2" of the boresighted LMXB position. Simultaneous *Rossi X-ray Timing Explorer* (*RXTE*) spectra, combined with the *Chandra* spectrum, indicate that EXO 1745-248 is an ultracompact binary system, and show a strong broad 6.55 keV iron line and an 8 keV smeared reflection edge.

Subject headings: X-rays: individual (EXO 1745-248) — X-rays : binaries — novae, cataclysmic variables — globular clusters: individual (Terzan 5) — stars: neutron

1. INTRODUCTION

The high resolution of the *Chandra X-ray Observatory* has enabled astronomers to study the low-luminosity X-ray source populations in globular clusters in great detail. Combined X-ray, radio, and optical *Hubble Space Telescope* (*HST*) studies of the globular cluster 47 Tucanae have revealed quiescent low-mass X-ray binaries (qLMXBs) that have not experienced X-ray outbursts in the history of X-ray astronomy, cataclysmic variables (CVs) as X-ray luminous as any known in the field, flaring behavior from coronally active stellar binary systems, and predominantly thermal X-ray emission from millisecond pulsars (MSPs) (Grindlay et al. 2001a, 2002). Similar populations have been uncovered in the globular clusters NGC 6397 (Grindlay et al. 2001b), NGC 6752 (Pooley et al. 2002a), and ω Cen (Rutledge et al. 2001, Cool, Haggard & Carlin 2002), while the luminosities and broad X-ray spectral types of these sources have allowed classification of sources in the more obscured cluster NGC 6440 (Pooley et al. 2002b) and M28 (Becker et al. 2003).

The globular cluster Terzan 5 contains a known transient LMXB, EXO 1745-248, which was first detected in a bursting state by *Hakucho* (Makishima et al. 1981), and has been irregularly active since then (Johnston et al. 1995 and refs. therein). EXO 1745-248 is one of the few luminous globular cluster LMXBs not analyzed by Sidoli et al. (2001; hereafter SPO01) or Parmar et al. (2001), who identify spectral distinctions between normal and ultracompact LMXBs. Ultracompact LMXBs, defined as having periods less than 1 hour, are thought to possess a degenerate helium white dwarf secondary. Deutsch et al. (2000) remark upon the overabundance of ultracompact LMXBs in globular clusters, and speculate that the short periods may be due to dynamical effects in globular clusters.

Terzan 5 also contains two identified MSPs, with many additional MSPs probably making up the extended steep-spectrum radio source at the cluster core (Lyne et al. 2000; Fruchter & Goss 2000). Terzan 5's high central density and large mass make it a rich target for studies of binary systems, but its high reddening and severe crowding make optical and even infrared observations extremely difficult. The deepest infrared survey of Terzan 5 was performed with the *HST* NICMOS camera by Cohn et al. (2002; hereafter CLG02). The extreme reddening indicates that the cluster parameters are best determined in the infrared. NICMOS observations produced the first CMDs of Terzan 5 to reach the main-sequence turnoff (CLG02; see also Ortolani et al. 2001). Therefore we utilize the new cluster parameters derived by CLG02 in our analysis, particularly the reddening, distance, core radius, and radial star-count profiles. The attempt by Edmonds et al. (2001, hereafter EGC01) to identify EXO 1745-248 and the eclipsing MSP through time-series variability analysis and color information did not uncover any promising candidates due to the crowding and overlapping Airy profiles, although it did identify two truly variable stars, one of which was shown to be an RR Lyrae variable.

This paper is organized as follows. Section 2.1 describes the observations we used. Section 2.2 explains our methods for detecting sources and performing an astrometric correction based upon identification of serendipitous sources. Section 2.3 describes our search for an infrared counterpart for EXO 1745-248, extending the work of EGC01 using our *Chandra* position. Section 2.4 classifies the faint X-ray sources, and quantifies our detection incompleteness (due to the outburst of EXO 1745-248). Section 2.5 attempts simple spectral fits to the faint sources, while section 2.6 examines the simultaneous *RXTE*

and *Chandra* spectra of EXO 1745-248. Section 3.1 compares our spectral analysis of EXO 1745-248 to other observations of LMXBs. Section 3.2 recalculates the central density and collision frequency of Terzan 5, while section 4 summarizes our conclusions.

2. ANALYSIS

2.1. *Description of Observations*

The *Chandra* X-ray Observatory observed the globular cluster Terzan 5 on July 24, 2000, for 45 ksec (05:46 to 18:22 TT), and on July 29, 2000 for 5 ksec (00:56 to 09:20 TT), with the ACIS-I instrument at the focus. Due to an error in the observation upload, both exposures were performed in 1/8 subarray mode (as intended for the shorter observation only), with frame times of 0.841 s (longer exposure with more chips) and 0.541 s. EXO 1745-248 entered an outburst during July 2000, its 2-10 keV flux varying between 54 and 600 mCrab during July and August, approaching its Eddington limit at maximum flux (Markwardt et al. 2000a, 2000b). *Rossi X-ray Timing Explorer* (*RXTE*) All-Sky Monitor (ASM) observations (results provided by the ASM/*RXTE* team[1]) show that the 2-10 keV countrate from EXO 1745-248 on July 24, 2000, was 5.3±0.9 cts s^{-1} ($\sim$ 72 mCrab) during our longer *Chandra* observation, rising to 9.8±0.9 cts s^{-1} in the second observation (Fig. 1).

Unfortunately, the *Chandra* observation of EXO 1745-248 was not optimized to study such a bright object (Fig. 2). The intense photon flux led to severe pileup, which occurs when two or more photons landing in the same or adjacent pixels between frames are recorded as a single event. Pileup can increase the energy of recorded events, or by altering the grade of the recorded event to a "bad" grade, cause the rejection of the event either before or after telemetry to the ground (See the *Chandra* Proposer's Observatory Guide, v.5, chapter 6). In this case the pileup was severe enough to cause the pre-telemetry rejection of all events recorded within $\sim$1" of the LMXB position. The LMXB's X-ray halo, by increasing the local background, greatly degraded our sensitivity to faint cluster sources. (The halo is due to a combination of dust grain scattering and the intrinsic breadth of the *Chandra* mirrors' point spread function.) Nevertheless, the spectacular resolution of *Chandra* did allow us to identify additional point sources up to 10^5 times fainter within 10" of EXO 1745-248. The readout streak (caused by photons from EXO 1745-248 arriving during the readout of the CCD) also degraded our survey, but we were able to extract a useful spectrum of EXO 1745-248 from the readout streak. We also analyzed a simultaneous *Rossi X-ray Timing Explorer* (*RXTE*) pointed observation from the HEASARC archive[2] (on July 24, 2000, 15:15 to 16:16 TT), for broad spectral coverage of the outburst of EXO 1745-248. The *HST* NICMOS data we used to search for a possible infrared counterpart to EXO 1745-248 are described in EGC01 and CLG02.

2.2. *Detection and astrometry*

We used the CIAO software package[3] to search for point sources, produce hardness ratios, and extract spectra and lightcurves. We reprocessed the two observations to remove the pixel randomization added in standard processing, and merged the two observations. No periods of high background flaring were observed. EXO 1745-248's X-ray halo displays an x-ray color (defined here as 2.5 log [0.5-1.5 keV counts/1.5-6 keV counts], following Grindlay et al. (2001a)) of -2.9, harder than most known faint globular cluster sources. Therefore, we selected a soft band, 0.5-2 keV, to search for point sources. We selected a 2.5×10^4 pixel (1.7 $arcmin^2$) square region including the cluster and ran WAVDETECT with the significance threshold set to give false positives at the rate of 10^{-4}. WAVDETECT indeed found two spurious sources (identified as spurious by eye, and by not appearing in more than one energy band) far from the cluster, as expected. Within three optical core radii (24") we identify nine point sources besides EXO 1745-248, each confirmed by visual inspection (see Figure 2) and with significance above 2.8 σ. We name the nine additional real sources in Table 1 with both positional names and simple reference names W2-W10 (used in the rest of this paper). Outside the globular cluster, we binned the remaining data into 1 arcsecond pixels and searched for back- or foreground serendipitous sources (setting the significance threshold to a false rate of 10^{-6}). We identified four sources that also pass visual inspection on the active portions (36 $arcminutes^2$) of the ACIS-I array. As they are all more than 2' (2.5 half-mass radii) from the cluster center, we hereafter identify them as "serendipitous sources". The ROSAT source S2 from Johnston et al. (1995) was not included in the field of view. Inspection of the locations of the known millisecond pulsars (A and C; Lyne et al. 2000) show no evidence of X-ray emission (using the astrometry below). The upper limits are 3 and 5 counts respectively in the 0.5-2 keV band, giving $L_X \leq 2 \times 10^{31}$ and $\leq 3 \times 10^{31}$ ergs s^{-1} for a power law of photon index 2. These are well above the X-ray luminosities of all identified millisecond pulsars in 47 Tuc (Grindlay et al. 2002), NGC 6397 (Grindlay et al. 2001b), and NGC 6752 (D'Amico et al. 2002), but below the luminosity ($L_X = 1.1 \times 10^{33}$ ergs s^{-1}) of the MSP B1821-24 in M28 (Danner et al. 1997). Soft thermal spectra give even less constraining limits, due to the high extinction. The two variables identified by EGC01 are also not seen, as expected based on their RR Lyrae and probable eclipsing blue straggler identifications.

Inspection of a Digital Sky Survey image reveals that one of the serendipitous sources has a probable optical counterpart. According to the Guide Star Catalog 2.2, a star with V=13.56, R=13.22 is located only 0.″36 from the position derived by WAVDETECT for the X-ray source that we name CXOU J174803.3-244854. This is consistent with the 0.″6 absolute astrometry (90% conf. radius) reported by Aldcroft et al. (2000) for *Chandra* . We estimate a probability of a positional coincidence within 0.″5 of one of the 15 brightest stars on the 7' by 7' survey plate with any of the four serendipitous X-ray sources of 8×10^{-5}. Another X-ray source (CXOU J174812.6-244811.1) has a faint star (R=16.8) 0.″14 away (when the frame is shifted to match star 1). We estimate the chances of a star this bright or brighter landing within 0.″5 of one of four *Chandra* sources as 4×10^{-3}. The other two X-ray sources show no stars in the GSC 2.2 Catalog within 3". We shift our *Chandra* frame by +0.^{s}004 in RA, and +0.″396 in Dec, to match the weighted

[1] See http://xte.mit.edu/.

[2] Available at http://heasarc.gsfc.nasa.gov/docs/corp/data.html.

[3] Available at http://asc.harvard.edu/ciao/.

[4] GSC 2.2 absolute astrometric errors, when compared to the international celestial reference frame, are of order 0.3-0.75 arcseconds; see http://www-gsss.stsci.edu/gsc/gsc2/GSC2home.htm.

GSC 2.2 star positions.[4]

The V and R magnitudes of star 1 suggest an F star, and the X-ray (0.5-2.5 keV) to V-band flux ratio (V-band flux defined as $10^{-0.4V-5.43}$ ergs cm^{-2} s^{-1}) is 2×10^{-4}, on the high end of values for nearby F stars (Hünsch et al. 1999). Star 2 has no color information in the GSC 2.2 Catalog. Assuming V-R$\sim$1.5 (appropriate for M2 stars) gives a flux ratio of 1×10^{-2}, which is common among M stars (Hünsch et al. 1999). The other two sources may be background AGN, or (perhaps more likely) CVs in the galactic bulge. Both show an Xcolor (2.5 log [0.5-1.5 keV cts/1.5-6 keV cts]) of -1.5, indicating strong absorption. Simple spectral fitting of the brighter source gives $N_H = 2.8^{+2.4}_{-1.2}\times10^{22}$ cm^{-2} for a powerlaw of photon index 1.7, as typical for AGN. A 10 keV bremsstrahlung spectrum (as for a bulge CV) would have $N_H = 2.7^{+2.5}_{-1.2}\times10^{22}$ cm^{-2}. The 2-10 keV log N–log S relation of Giacconi et al. (2001) suggests that 1-3 AGN may be expected at these observed flux levels in our ACIS-I subarray field (although the location of detected sources near to the aimpoint suggests that our sensitivity is not uniform across the field). Recent results from galactic bulge surveys (Grindlay et al. 2003) indicate that bulge CVs or compact binaries outnumber AGN at these flux levels, suggesting that these two sources may be bulge CVs.

We found the position of EXO 1745-248 by centering the symmetric "hole" caused by extreme pileup and the readout streak. We estimate our error in this determination at 2/5 of a pixel, or 0.″2. We present the positions (in the GSC 2.2 frame) of EXO 1745-248, the nine additional globular cluster sources, and the four serendipitous sources (with relative positional errors from WAVDETECT) in Table 1, along with the background-subtracted counts in three bands.

2.3. *Identification of plausible infrared counterpart to EXO 1745-248*

Our refined position for EXO 1745-248 allowed us to undertake a careful search of the small *Chandra* error circle in the June 1998 *Hubble Space Telescope* NIC2 F110W and F187W data, for which the photometric analysis is described in EGC01. We estimate an error of 0.″1 in the shift to the GSC 2.2 frame, based on the scatter of the two stars used in the boresighting. An additional error of 0.″37 (following EGC01) is incurred in the shift between the GSC 2.2 and *HST* NICMOS frames. Combining these with the 0.″2 centering positional uncertainty gives an error for the position in the NICMOS frame of 0.″4. This error circle is fortuitously free of bright red giants. Error circles for six other X-ray sources in the cluster lie wholly or partially within the NIC2 field of view.

Comparison of the F110W and F187W images with a ratio image (Figure 3) shows a significantly blue faint star (hereafter star A) within the *Chandra* error circle, only 0.″2 from the corrected position of EXO 1745-248. A combination of this star and another star just above it (Star B) was shown in the cleaned CMD of EGC01 (their figure 8) as one of only two stars that lie more than 3σ to the blue from the distribution of stars in that color-magnitude diagram. Our attempts at separate PSF-fitting using ALLSTAR in DAOPHOT encountered two problems: (1) we were unable to fit stars A and B simultaneously and (2) the sky-fitting component in PHOT and ALLSTAR gave local sky (background) values that were too high, because stars A and B are surrounded by a ring of bright stars. The latter is a formidable problem in this crowded field, especially in F187W where the background contribution of neighboring red giants is greater than in F110W.

We therefore adopted a customized procedure to estimate the F110W and F187W magnitudes for stars A and B. For sky determination we adopted the mean of the two 2-by-2 pixel regions having the lowest intensity values within an 8 pixel radius of star B. Using the F110W and F187W images, and the ratio image, we determined the positions of stars A and B. Using PSF models and the DAOPHOT program ADDSTAR to create models for stars A and B we subtracted these models from the two images to produce residual images, while keeping the positions of stars A and B fixed. Since no other close-by stars are obviously present, stars A and B are accurately modeled if the mean aperture counts (after subtracting the sky) at their positions in the residual image are equal to zero. We iteratively varied the magnitudes of these two stars until this goal was met. The results of these fits are shown in the lower right-hand corner of Figure 3. Clearly the subtractions of stars A and B were successful, given the relatively smooth residuals.

We performed aperture photometry on the residual images to produce photometry that is consistent with Figure 8 of EGC01. Photometry for stars A and B were measured by subtracting off stars B and A respectively, and the results are shown in Figure 4. Variables 1 and 2 from EGC01 are labeled with crosses, and stars within 1" of X-ray sources are circled. The main-sequence turnoff (not reached at the cluster core) is at F110W$\approx$ 20 (CLG02). Note the apparently blue color of star A ($\sim 2.5\sigma$ from the subgiant sequence) lying near the top of the blue straggler sequence. The error in the color of star A is dominated by the error in the F187W magnitude. The high sky background in F187W caused the original F187W magnitude determination for the combination of stars A and B to be too low, and thus shifted the combination bluewards. Our customized procedure thus gives redder colors for both stars A and B than the original determination for the combination.

Given the blue appearance of star A in both the normal and residual images, the reasonable evidence for blue colors in our photometric analysis, and its proximity to the center of the X-ray error circle, star A is a reasonable candidate for the IR counterpart to EXO 1745-248. No evidence is seen for statistically significant variability of star A, but the faintness of star A and its strong blending with star B limits the depth of variability searches. Only the F110W images are useful for time series analysis, and only sparse coverage was obtained here over 1.16 days. Images in the *V* and *I* passbands with the Advanced Camera (in High Resolution mode) on *HST* should do a much better job of separating stars A and B and would provide much better constraints on variability if taken at several different epochs near outburst and quiescence.

Since the F187W band does not correspond to any ground-based filter, standard calibrations for it do not exist. We apply rough transformations to estimate interesting quantities. We estimate the unreddened J magnitude from the F110W and F187W magnitudes by the equation

$J_0 = F110W + 0.033 - 0.178(F110W - F187W) + A_J$

derived assuming that the spectral slope is constant over this range. Using A_J/A_V=0.282 and A_V=6.75 (CLG02), we find J_0=16.40, M_J=1.7. We calculate the color (F110W-F187W)$_0$= -0.17 ± 0.3. Assuming that the photometry is accurate, three alternatives to an LMXB nature remain for this star: it could be a blue horizontal branch star, it could be a blue straggler, or it could be a foreground star. We plot simple interpolated blue straggler and horizontal branch sequences in Figure 4. Star A's

position may be consistent with that of a blue horizontal branch star, although a blue horizontal branch has only been hinted at in Terzan 5 (CLG02). It is also consistent with an extremely heavy (more than twice the turnoff mass) blue straggler, or a blue straggler binary (as variable 2 from EGC01, plotted as an "X" next to star A in figure 4, may be). The other extremely blue star seen in Figure 4 is probably a foreground star, which also cannot be excluded as a possibility for star A. However, the chance of one of the five bluest stars in the 19.″2 square NIC2 FOV landing in the 0.″4 error circle by chance is only 7×10^{-3}. None of the stars in the other X-ray error circles (circled in Figure 4) display any unusual colors or variability. This is expected based upon the magnitudes of CVs and quiescent LMXBs, in the field and other globular clusters, which very rarely reach the turnoff magnitude (Grindlay et al. 2001a, b, Pooley et al. 2002a).

We compare this suggested counterpart to other low-mass X-ray binaries observed in the infrared by calculating the ratio of X-ray to infrared luminosity. Using the ASM lightcurve in figure 1, we see that the average ASM countrate for the 11 days leading up to the *HST* observation was 1.5 ± 0.2 cts s^{-1}, compared to 5.3 ± 0.9 cts s^{-1} at the time of the *Chandra* observation. The high source confusion near the galactic center for the ASM makes this data relatively noisy, so we take 1.5 cts s^{-1} as an upper limit on the X-ray flux. Assuming the same spectrum as we find in 2000 (see Sect. 2.5), we derive an unabsorbed 0.5-10 keV X-ray flux of 6.1×10^{-10} ergs cm^{-2} s^{-1} and an unabsorbed J-band flux of 1.2×10^{-13} ergs cm^{-2} s^{-1}, thus $\log(L_X/L_J) \leq 3.7$. We note that van Paradijs and McClintock (1995) find $\log(L_X(\text{2-11 keV})/L_{Opt}(\text{3000-7000 Å})) \sim 2.7$ for typical bright LMXBs.

Rough $(J-K)_0$ colors have been reported for the soft X-ray transients in outburst QX Nor, or X1608-52 ($0.5 < (J-K)_0 < -0.4$, Wachter 1997), and SAX J1808.4-3658 (0.1 ± 0.1, Wang et al. 2001) and the faint LMXB X1323-619 (-0.1 ± 1.4, Smale 1995). Our value of (F110W-F187W)$_0 \sim -0.17 \pm 0.3$ for star A, implying $(J-K)_0 \sim -0.3$, is consistent with this broad range. Infrared colors observed by Wachter (1998) give an even broader range ($-0.4 < (J-K)_0 < 1.41$), as some LMXBs are dominated by the disk light in the IR, while others are dominated by the light of the secondary. This makes identification of LMXBs by infrared colors very difficult, and leaves our identification uncertain.

2.4. *X-ray Classification and Completeness*

We extracted the numbers of counts within 1" radius of the sources (containing 90% of source flux at 1.5 keV[5]) in the 0.5-1.5, 0.5-4.5, and 1.5-6 keV bands. We then subtract 1/3 (ratio of areas) of the counts from background 1"-2" annuli around these sources for each band (except where the annuli would overlap with other sources, where we offset the extraction region). The results are listed in Table 1. Constructing an X-ray CMD (as in GHE01a; Xcolor is defined as 2.5 log[0.5-1.5 keV counts/1.5-6 keV counts], while the vertical axis is log[0.5-4.5 keV counts]), we are able to identify two populations of faint sources with distinct X-ray colors. Using an N_H of 1.2×10^{22} cm^{-2} (derived from CLG02's estimate of A_V=6.75, using Predehl & Schmitt's (1995) conversion factor), we apply a uniform shift to the coordinates of the CMD as Pooley et al. (2002b) do for the moderately reddened globular cluster NGC 6440. The identified dim sources (and the color of the LMXB halo, which determines the background) are plotted in the upper panel of Figure 5. The upper and right axes show the raw (absorbed) Xcolor and counts, while the lower and left axes represent the corrected (unabsorbed) Xcolor and counts. (We note that the interstellar medium decreases soft fluxes more than hard fluxes. Thus this simple shift of axes should be used with caution.) Another version of the same diagram, but plotting luminosities derived from spectral fits (section 2.5 below) against corrected Xcolor as above, is shown in the lower panel of figure 5. Errors on the vertical axis are derived from errors in the counts, and do not include spectral uncertainties. This version of the diagram (inspired by Becker et al. 2003), is more useful for comparing different clusters, but is dependent on spectral and reddening assumptions. The luminosities of the two populations roughly agree with the range observed for their respective counterparts in 47 Tuc and NGC 6440. This suggests that the soft population (W2, W3, W4, W8) should be identified with qLMXBs containing neutron stars and that the harder population is composed of bright CVs.

We estimate our incompleteness, due to the X-ray halo and streak from the LMXB EXO 1745-248, by the use of artificial-star tests. We generated uniform grids of artificial point sources at different luminosities using the MARX software[6] and merged the simulated data with our 0.5-2.0 keV master image to see if we could detect the fake sources. We scaled the average (Poisson-distributed) counts of the artificial sources to the average detected counts of real sources for which XSPEC fitting gave the target luminosity (see section 2.5 below). E.g., for $L_X = 10^{32}$ erg s^{-1} sources, the average number of counts per simulated source was 20, and for $L_X = 3 \times 10^{32}$ erg s^{-1} it was 45 counts. (The counts-luminosity relation varied depending on the kind of sources prevalent at different luminosities.) We performed the tests for artificial source 0.5-2.5 keV luminosities of 10^{32}, 1.7×10^{32}, 3×10^{32}, and 10^{33} ergs s^{-1}, assuming spectra similar to the average of our detected sources. We separated the artificial sources by 5" so that each source would suffer only the crowding that exists in the real data. We merged grids of point sources with the Chandra image four times for the 10^{32} and 1.7×10^{32} tests, and three times for the other two tests, shifting the grids by several arcseconds between each trial. We then applied WAVDETECT to each image, keeping the same parameters as in section 2.2. We counted the number of artificial sources that landed within one optical core radius, between one and two core radii, and between two and three core radii for each trial, and the number of sources detected in each region, for a total of $\sim$1000 point-source trials. We note that this approach takes crowding into account, in that the test sources will be crowded by any real undetected sources. Parts of the 1-2 core radii annulus and 2-3 core radii annulus were imaged only in the 5 ksec exposure and not in the 42 ksec exposure. The 2-3r_c bin also includes a small area that is completely unexposed (due to the use of the subarray). We scaled the MARX point source luminosities appropriately and performed separate trials for the low-exposure regions (where sources below 3×10^{32} ergs s^{-1} were never detected), and then included these results in the total completeness calculations. This allowed an incompleteness factor to be determined for each radial annulus for each of four luminosity bins, which we created by equally dividing (in a logarithmic sense) the ranges between our test luminosities.

[5] CXC Proposer's Observatory Guide, http://cxc.harvard.edu/udocs/docs/docs.html

[6] Available at http://space.mit.edu/ASC/MARX.

The number of real sources detected was too small to effectively determine both a radial distribution and a luminosity function (1 source within 1 r_c, 5 within 1-2 r_c, 3 within 2-3 r_c). Therefore we assumed a luminosity function of the form $dN \propto L^{-\gamma} d\ln L$, $L > L_{\rm min}$ following Johnston & Verbunt (1996). We fixed γ at 0.5 first, as found for sources between 10^{32} and 10^{33} ergs s^{-1} in NGC 6440 (Pooley et al. 2002b) and the general globular cluster system (Johnston & Verbunt 1996), and then allowed γ to vary within the range 0.29 to 0.78 found by Pooley et al. (2002b). The uncertainty in our incompleteness due to different possible values of γ was small compared with errors due to small-number statistics. For each annulus, we determined an average incompleteness factor using the results of our testing and the weights derived from the luminosity function for the luminosity bins as specified above.

To calculate how many sources were missed, we take the number of sources detected in each annulus and apply the 1σ errors for small numbers given by Gehrels (1986). These numbers and errors are multiplied by 1/f, where f is the completeness fraction, to obtain the average density of sources in each annulus. Then we calculated the expected numbers of missed sources, using the estimated density and again applying small-number errors. We ignore possible systematics in the method, since the random errors are so large. Thus, above 10^{32} ergs s^{-1}, we find that within 1 r_c we predict $0.8^{+2.8}_{-0.8}$ additional sources, within 1-2 r_c we predict $1.5^{+2.8}_{-1.3}$ additional sources, and within 2-3 r_c we predict $1.1^{+2.6}_{-1.0}$ sources, giving a total probable number of $11.4^{+4.7}_{-1.8}$ sources between 10^{32} and 10^{33} ergs s^{-1} in Terzan 5. We note that this source population is very similar to the 11 sources in this flux range identified in NGC 6440 (Pooley et al. 2002b), as expected considering the similar cluster parameters (as derived in section 3.2 below).

The radial distribution we infer can be compared with that predicted by a "generalized King model" (Lugger, Cohn, & Grindlay 1996) where the surface density of sources varies as

$S_x(r) \propto [1+(\frac{r}{r_c})^2]^{\frac{\alpha_X}{2}}$

where $\alpha_X = -(3q-1)$ and $q = \frac{<m_x>}{<m_*>}$, the ratio of the average X-ray system mass to the mass of the stars that dominate the density profile (i.e., turnoff-mass stars for King model clusters). The soft sources in 47 Tuc (thought to be largely MSPs) have $\alpha_X = -3.6$ and the CVs in 47 Tuc have $\alpha_X = -3.1$ (Grindlay et al. 2002). Comparing the corrected source counts in each annulus with the predictions of generalized King models with $\alpha_X = -2$, -3, and -4, we find a best fit with $\alpha_X = -2$, suggesting similarity in source mass to the turnoff mass stars. However, the large uncertainties on our source numbers (especially in the core) allow consistency with $\alpha_X = -3$ in a χ^2 sense. We conclude that the small number of sources does not allow a sensitive test of the radial distribution, and thus of the mass of the X-ray sources. Upcoming *Chandra* observations of Terzan 5 (PI: R. Wijnands) should identify more X-ray sources, allowing a better probe of the luminosity function and radial distribution.

2.5. *Spectral fitting and variability of faint sources*

We extracted the spectra of the detected X-ray sources (except for EXO 1745-248; see section 2.6) from 1" radius circles around the wavdetect positions, with background spectra taken from 1-2" annuli, using the *psextract* CIAO script. We utilize the recently released ancillary response file correction[7] for the time-variable low-energy quantum efficiency degradation in all spectral fits in this paper. This correction had a very small impact on our fits (in part because of the large N_H). We group the spectra with at least 10 counts/bin, and fit models in XSPEC (Arnaud 1996), all using the near-infrared-derived value of photoelectric absorption (CLG02). The models used were thermal bremsstrahlung, a powerlaw, and a hydrogen atmosphere appropriate for an accreting neutron star in quiescence (Lloyd 2003). Simple background subtraction is not the preferred way to fit spectra from sources with high background, due to deviations from Poisson statistics in the subtracted counts. We verified that Sherpa spectral fitting of source and background simultaneously gives results within the errors of our XSPEC analysis where we are able to use the same models, but note that these low signal-to-noise spectra should be taken with caution.

A thermal bremsstrahlung spectrum of kT$\gtrsim$5 keV seems to describe most cataclysmic variables in the globular clusters 47 Tuc and NGC 6397 (Grindlay et al. 2001a,b). We fixed the normalization of the hydrogen atmosphere models, set to (r [km]/D[10 kpc])^2= 132 (appropriate for a 10 km neutron star at 8.7 kpc), and the redshift to 0.306. This tests for compatibility with a canonical 1.4 $M_\odot$, 10 km neutron star. A hard power law component has been found to dominate qLMXB spectra above 2-3 keV in some systems, but has not yet been identified in globular cluster qLMXBs that have not displayed outbursts (see Heinke et al. 2002). We make no attempt to confirm or rule out such a hard component in this paper due to the extremely high background (from EXO 1745-248) above 2 keV.

The results of our spectral fitting are shown in Table 2 (errors are 90% confidence). All of the four sources on the right side of the X-ray CMD (W2, W3, W4, W8) are well fit by our hydrogen atmosphere model. Alternative models require steep powerlaw spectra ($\alpha > 2$) or bremsstrahlung temperatures below 2 keV, not seen in bright ($> 10^{32}$ ergs s^{-1}) CV or millisecond pulsar systems (Grindlay et al. 2001a, 2001b, 2002, Pooley et al. 2002a). Their high luminosities of $3-6\times10^{32}$ ergs s^{-1} and soft spectra rule out flaring coronal events from BY Dra or RS CVn binary systems (see e.g. Grindlay et al. 2001a). Therefore we conclude that these are probably qLMXB systems. The five sources on the left of the CMD (W5, W6, W7, W9, W10) are well fit by bremsstrahlung spectra with kT$>$5 keV, or power law spectra with α=1.0-1.6, and are not acceptably fit by hydrogen atmosphere models with the normalization fixed to a 10 km radius. We conclude that these are most likely highly X-ray luminous cataclysmic variables, though MSPs and RS CVn stars are (less likely) possibilities.

We test for variability by extracting the events files between 0.5 and 2.5 keV within 1" of each source, and using the IRAF PROS task `vartst`. This task applies the Kolmogorov-Smirnov and Cramer-Von Mises tests (Daniel 1990) to attempt to disprove the hypothesis that the source flux is constant. We choose only events below 2.5 keV because the events at higher energies are generally dominated by the background from EXO 1745-248. Only two sources are found to be significantly variable in both tests, W9 and W10 (identified as probable CVs above). Both are variable with 99% confidence. This is consistent with the trend for qLMXBs of $L_X \sim 10^{32-33}$ ergs s^{-1} to show generally constant flux, compared to globular cluster CVs that are often highly variable (Grindlay et al. 2001b, Heinke et al. 2002, but cf. Becker et al. 2003).

[7] See http://cxc.harvard.edu/cal/Links/Acis/acis/Cal_prods/qeDeg/index.html.

2.6. *Spectral fitting of EXO 1745-248*

When observed by the ROSAT All-Sky Survey at a luminosity of log(L_X)=35.3, the 0.5-2.5 keV spectrum of EXO 1745-248 was well fit by a powerlaw of photon index α=1.2, using a hydrogen column of $N_H = 2 \times 10^{22}$ cm^{-2} (Verbunt et al. 1995). A ROSAT HRI observation in March 1991 found it at a luminosity of log(L_X)=34.6, assuming the same spectrum (Johnston et al. 1995). Only a broad-band X-ray spectrum can provide detailed information about the nature of the LMXB, by simultaneously constraining the photoelectric absorption column, any iron lines or edges, and the overall spectral shape. Fortuitously, there exist *RXTE* data simultaneous with our *Chandra* data, which we also analyze.

To study the *Chandra* spectrum of EXO 1745-248 in outburst, we first selected an annulus from 5 to 9 arcseconds from our best-determined position, and removed the portion affected by the readout streak. This annulus is not affected by pileup, and includes only one faint source (W4) which should not significantly affect the spectral fitting (contributing $\sim$ 17 of 24739 counts). We extracted the spectrum using bins of width 75 eV (oversampling the energy resolution) and using a background region on the same chip 2' away. We also extract a lightcurve from the same region. We see a gradual rise from 0.4 counts s^{-1} to 0.5 counts s^{-1} during the first observation, while the second (5 ksec) observation five days later shows a rate of 0.9 counts s^{-1} (consistent with the rise in the ASM countrate). Flickering is clearly seen, but we put off detailed study of temporal variability for future work. An absorbed powerlaw of photon index 0.24 provides a good fit to the continuum, with a strong broad iron line (EW 440^{+190}_{-230} eV, $\sigma = 0.5 \pm 0.1$ keV) required at 6.7 keV. However, we note that the spectrum will be altered both by the effects of dust scattering and by the energy dependence of the *Chandra* mirror psf (e.g., Smith, Edgar & Shafer 2002). Therefore we extracted the spectrum from the readout streak, which does not suffer this hardening since the counts are recorded in the image core.

We used the CIAO task *acisreadcorr* to identify and reposition events in the EXO 1745-248 readout streak. We use a strip of width 2 pixels and omit a region of 25 pixels radius around the source location, to avoid photons from the X-ray halo and regions that suffered pileup. Pileup is not an issue in the selected region, as the 8750 counts selected give 0.15 cts (0.841 s CCD frame)$^{-1}$, spread along a 78$\times$2 pixel column. We extracted those events using the CIAO script *psextract*, and chose a background region adjacent to the strip (adjusting the BACKSCAL parameter by hand). We ignore data above 10 keV and below 0.7 keV (which is almost entirely background photons, considering the high absorption to this source). We fit this *Chandra* readout streak spectrum along with the simultaneous *RXTE* data to understand the full spectral shape.

From the *RXTE* data, only the PCA STANDARD 2 data and the HEXTE Archive data (from both HEXTE clusters separately) are analyzed in this paper. We choose time intervals when three of the PCA units were on (the maximum during the observation) and the elevation above the earth's limb was greater than 10 degrees. Selecting only the top xenon layer data from the PCA, we use PCABACKEST version 3.0 (released Feb. 1, 2002) and PCARSP version 8.0, and correct the PCA data manually for deadtime. We used the HEXTE response matrices hexte_97mar20c_pwa.rmf and hexte_97mar20c_pwb013.rmf, and corrected the HEXTE data for background and deadtime using the HXTBACK and HXTDEAD (version 2.0.0) scripts. We eliminate 200 seconds around a possible Type I X-ray burst, which we do not investigate in this paper (Type I bursts are common from EXO 1745-248; see Inoue et al. 1984). This gave total corrected exposure times of 2060, 731, and 777 seconds for the PCA and HEXTE clusters A and B respectively. We analyze PCA data from 3 to 25 keV, and HEXTE data from 25 to 125 keV. Following Barret et al. (2001), we add systematic errors of 0.5% to the PCA data below 15 keV, and 1% to PCA data above 15 keV using the FTOOLS GRPPHA. We leave an overall normalization free between the *Chandra* , PCA and HEXTE data, but link all other parameters between them in a joint fit. (The PCA and HEXTE relative normalizations are generally not well-calibrated; we find the HEXTE normalization to be 40% lower than the PCA normalization.)

The standard models for fitting neutron star LMXB spectra are an absorbed multicolor blackbody, or a simple blackbody, with an additional hard component due to comptonization of soft photons by hot electrons (generally assuming, as here, a spherical geometry); see Barret et al. (2000), and Sidoli et al. (2001). Fitting a simpler model to the RXTE data, consisting of DISKBB plus a gaussian and powerlaw, gave a photon index of 1.5, but failed to fit the HEXTE data due to a dropoff of flux at high energies (χ^2_ν=8.1 for 230 degrees of freedom). We begin by fitting our *RXTE* spectra with a model consisting of an absorbed multicolor blackbody (DISKBB; Makishima et al. 2000), a comptonization model (COMPTT; Titarchuk 1994), and the Fe-line gaussian, and with another model consisting of a blackbody, COMPTT, and the gaussian. The *RXTE* fits for both models are significantly improved by the addition of a smeared iron edge ("smedge"; Ebisawa et al. 1994) near 8 keV, as expected for reflection of Comptonized hard X-rays from a disk. (An F-test gives a probability of 10^{-4} that the smeared edge is not needed.) For the rest of this analysis, the "standard model" shall refer to PHABS(DISKBB + COMPTT + GAUSSIAN)*SMEDGE*CONSTANT. The data/model ratio for PCA data, fit with the standard model with the normalizations of the gaussian and smeared edge set to zero, are shown in Figure 6.

The *Chandra* spectrum extracted displays what appear to be emission lines at $\sim$1.95 and 2.1 keV. These features are not apparent in either the adjacent background, or the annulus spectrum described above. Similar features are also seen in the readout streak spectrum of GX 13+1 (Smith et al. 2002), and in the high count rate continuous-clocking spectrum of RX J170930.2-263927 (Jonker et al. 2003). The best-fitting standard model to the *RXTE* data does not give an acceptable fit to the *Chandra* data above 5 keV, where they overlap, nor does any other model fit both the *Chandra* and *RXTE* data; see Figure 7. For the best-fit standard model, the reduced χ^2=1.41 for 225 degrees of freedom (null hypothesis prob.=5.7×10^{-5}). Note that the *Chandra* spectrum appears to have been shifted in energy compared to the model predictions. We understand this effect as being due to a gain shift between the calibrated response of the timed exposure mode, and the actual response to events occurring during the readout period, when the voltages in the CCD are expected to be different. By measuring the difference between the model and data edges near 2 keV, and the model (derived from *RXTE* fits) and data between 5 and 9 keV, we estimate the gain shift at 7$\pm$1%.

We attempt to compensate for this gain shift by increasing the size of the energy bins in the events file by 7%, to 15.6 eV from 14.6 eV, while keeping the same response, ancillary

response, and background files and extracting the altered-gain spectrum in the same way. Fitting this shifted-energy spectrum, along with the *RXTE* spectra, gives a greatly improved fit (see Figure 8). The standard model fit to these spectra gives a reduced χ^2=1.06 for 225 dof (prob=0.250). The derived parameter ranges are robust; spectral fits to *RXTE* data alone give similar parameter values (with larger uncertainties for the soft components, and N_H virtually unconstrained). Although this simple calibration must be used with a great amount of caution, we believe that the quality of the resulting spectral fits supports our decision to utilize it for this analysis.

We list the best-fitting parameters (and 90% confidence errors) for the two models in Tables 3 and 4, along with the derived values for the radii of the thermal components and the ratio of luminosities in the two components *f*. We have not corrected the multicolor disk-blackbody spectral parameters for the spectral hardening factor expected in high accretion rate systems (see Shimura & Takahara 1995, Merloni et al. 2000), for ease of comparison to the work of SPO01 and Parmar et al. (2001) below. The averages of the best-fit luminosities (from the two fits' PCA normalizations) are L_X(0.5-10)=2.1×10^{37}, and L_X(0.1-100)=6.6×10^{37} ergs s^{-1}. Several authors (e.g. Bloser et al. 2000) have commented upon an absolute uncertainty in the PCA flux normalizations of order 15%, which we do not attempt to compensate for. We note that the ranges of N_H required by these fits (1.3–1.9 $\times 10^{22}$ cm^{-2}) are slightly larger than the infrared-derived estimate of CLG02, 1.2×10^{22}, indicating probable internal absorption in the LMXB system.

3. DISCUSSION

3.1. *Ultra-compact nature of EXO 1745-248*

We compare our results from fitting combined *Chandra* and *RXTE* data with our "standard model" spectrum, to the spectral fits of SPO01 and Parmar et al. (2001) for the other globular cluster LMXBs, observed with BeppoSAX. Five comparisons using the DISKBB + COMPTT model in SPO01 separate the "normal" (not ultra-compact) globular cluster LMXBs in Terzan 2, NGC 6440, NGC 6441, and Terzan 6 from the ultracompact (binary periods $<$ 1 hour) LMXBs in NGC 6624, NGC 1851, NGC 6712, and (probably) NGC 6652. SPO01 note that these comparisons suggest that the DISKBB model is physically meaningful only for the ultracompact LMXBs.

• The ultracompact LMXBs show an inner DISKBB temperature below 1 keV, while the normal LMXBs show kT_{in} between 1.9 and 3.5 keV. EXO 1745-248 shows $kT_{in} = 0.80^{+.38}_{-.16}$ keV.

• The seed photon temperature kT_0 for the ultracompact binaries is roughly equal to the inner DISKBB edge temperature, while for the normal LMXBs the seed photon temperature is 4–5$\times$ lower. EXO 1745-248 seems to have similar values for kT_0 ($1.29^{+.40}_{-.13}$ keV) and kT_{in} ($0.80^{+.38}_{-.16}$ keV).

• The inferred inner radius R_{in} (cos i)$^{0.5}$ of the normal LMXBs is very small (0.3 to 1 km), while for the ultracompact LMXBs it is 3 to 45 km. EXO 1745-248's implied R_{in} (cos i)$^{0.5}$ is $8.7^{+5.0}_{-4.4}$ km.

• The seed photon emission radius $R_W = 3 \times 10^4 d \sqrt{f_{comptt}/(1+y)}/(kT_0)^2$ km, where d is the source distance in kpc, f_{comptt} is the luminosity in the Comptonized component in ergs cm^{-2} s^{-1}, and y is the COMPTT Comptonization parameter, $y = 4kT_e\tau^2/m_ec^2$. R_W is similar to the inner disk radius R_{in} (cos i)$^{0.5}$ in the ultracompact LMXBs, while it is $\sim$10-50$\times$ larger for the normal LMXBs. For EXO 1745-248 we calculate R_W=$5.4^{+1.3}_{-2.9}$ km, similar to its R_{in} (cos i)$^{0.5}$ = $8.7^{+5.0}_{-4.4}$ km. (We also note that $y = 5.2^{+0.5}_{-0.6}$ for EXO 1745-248, within the range 1-7 of most of the LMXBs studied in SPO01).

• Finally, the implied mass of the compact object, derived from the DISKBB extrapolated bolometric luminosity and the inner disk temperature (following Makishima et al. 2000, including spectral hardening), is consistent with 1-3 $M_\odot$ for the ultracompact binaries, but is nearer 0.1 $M_\odot$ for the normal LMXBs. We derive $1.6^{+0.8}_{-0.9}$ $M_\odot$ for EXO 1745-248.

Each of these comparisons strongly indicates that EXO 1745-248 is an ultracompact LMXB. Some of these spectral differences have been used by Parmar et al. (2001) to identify the bright LMXB in NGC 6652 as a probable ultracompact system, which is supported by the short optical periods proposed by Heinke et al. (2001). The identification of EXO 1745-248 as a probable ultracompact LMXB makes five of 13 luminous LMXBs in globular clusters ultracompact, a far greater proportion than in the field. This strengthens the conclusion of Deutsch et al. (2000) that dynamical effects are probably responsible for the generation of ultracompact LMXBs in globular clusters.

Another interesting result is the strength of the ionized iron line in EXO 1745-248, with an equivalent width (EW) $\sim$ 190 eV. This is many times larger than the average upper limit (25.6 eV) on the equivalent width of an iron line for the nine globular cluster LMXBs with good statistics reported by SPO01 and Parmar et al. (2001). Only two other globular cluster LMXBs have identified iron lines; 4U 1820-30 in NGC 6624 (EW=13^{+12}_{-11} eV, SPO01; EW=31^{+12}_{-11} eV at 6.6 keV, Asai et al. 2000; EW=27-94 eV in numerous *RXTE* observations, Bloser et al. 2000) and Terzan 2 (EW 21^{+10}_{-9} or 27$\pm$10 eV depending on continuum model, Barret et al. 2000). Among these LMXBs, only 4U 1820-30 in NGC 6624 has a reported reflection edge feature (at 7.7 or 8.9 keV; Bloser et al. 2000), in its low or "island" state. The strength of the iron line may be increased by the high metallicity of Terzan 5, suggested by CLG02 to be greater than solar, compared to the significantly subsolar metallicity for the other globulars with LMXBs except Liller 1. We note that the $6.55^{+.06}_{-.07}$ keV energy and $\sigma = 0.31^{+.16}_{-.15}$ keV breadth of this line are similar to those of field neutron star LMXBs reported in Asai et al. (2000), 6.56 keV and 0.2$\pm$0.1 keV (0.5 keV FWHM) respectively, although this line is somewhat stronger than in most field LMXBs. The iron lines studied by Asai et al. (2000) were interpreted as radiative recombination in an accretion disk corona, with the breadth being due primarily to Compton scattering, with possible small contributions from Doppler shifts (due to Keplerian motion near the NS) and line mixing from plasmas in different ionization states. The location of our line and smeared edge suggest iron that is less highly ionized than He-like Fe XXV K lines (6.68 keV line and 8.8 keV edge). Disk reflection from carbon-like Fe XXI (6.54 and 8.3 keV line and edge) is more consistent with our line and edge energies. Further analysis of the *RXTE* outburst spectrum and variability of EXO 1745-248 is being performed by Homan et al. (in preparation).

Kuulkers et al. (2002) have recently presented a BeppoSAX spectrum of EXO 1745-248, taken 15 days later during the same 2000 outburst. Kuulkers et al. (2002) find an interstellar absorption of $N_H = 3.8^{+0.9}_{-0.7} \times 10^{22}$ cm^{-2} when using the DISKBB + COMPTT model, and $N_H = 2.3^{+0.6}_{-0.8} \times 10^{22}$ using the BBODYRAD +COMPTT model. These values are inconsistent with our (more precise) values for N_H, suggesting that the absorption column may have changed during the outburst. Their

N_H values are inconsistent with the optically derived extinction value (CLG02; see figure 1 in Kuulkers et al. 2002), requiring an absorption column within the LMXB system ten times larger than shown in any other globular cluster LMXB. If this were the case, we would expect a high inclination and significant dips due to variable absorption. While these are not seen in our Chandra and single-observation *RXTE* lightcurves, R. Wijnands notes (priv. comm.) that such dips are indeed seen in the full *RXTE* lightcurves of EXO 1745-248's 2000 outburst (J. Homan, in prep.). This may imply that the system is at high inclination, though the observed disk reflection component suggests a low inclination. We also note that their spectral parameters, while not agreeing with ours in every detail, support our claim that EXO 1745-248 is ultracompact, particularly in their small value of kT_{in} for their DISKBB + COMPTT fit.

3.2. *Terzan 5 cluster parameters*

It has long been suspected that Terzan 5 has one of the highest rates of close encounters between stars of any Galactic globular cluster. The "collision rate", or rate of close encounters given by $\Gamma \propto \rho_0^2 r_c^3/\sigma$ (where ρ_0 is the central density, r_c is the core radius, and σ is the central velocity dispersion), is expected to predict the relative rates of formation of accreting binary neutron star systems by two-body encounters (Verbunt & Hut 1987). Thus, the similar numbers of X-ray sources in NGC 6440 and Terzan 5 might seem a surprise, as Terzan 5 has been predicted to show three times as many collision products as NGC 6440 and 17% of the total of such objects in the Galactic globular system (Verbunt 2002).

Our calculation of the central density of Terzan 5 uses the extinction-corrected central surface brightness $\mu_V(0)$ = 20.5, combining the star-count profile of CLG02 for the inner core with the surface brightness profile of Trager et al. (1995) for normalization beyond 10". We use the central concentration parameter c=2.0, core radius r_c=7.″9, heliocentric distance of 8.7 kpc, and A_V=6.75 from CLG02, as well as M_V = –7.91 from the updated Harris (1996; rev. 1999) catalog. Following the prescription of Djorgovski (1993), our result is that Terzan 5's central density is $1.7 \times 10^5 L_\odot$ pc^{-3}, significantly less than given by Djorgovski (1993), Harris (1996), or CLG02. The former two studies used a larger value of A_V, which produces a larger correction of the surface brightness. CLG02 had scaled the central surface brightness value of Djorgovski (1993) for changes in the profile, without updating the value of A_V. We note that this calculation is consistent with the lower limit of 5.0×10^5 $M_\odot$pc^{-3} derived by Lyne et al. (2000) from the acceleration-induced $\dot{E}$ of pulsar Terzan 5 C, provided that M/L$\geq$ 3.0. Using this central density, and the distance and core radius from CLG02, the collision rate in Terzan 5 is similar to that in NGC 6440 (5.9% of the total collision rate in the globular system), instead of three times larger. This is consistent with the results of our artificial star tests (section 2.3), which suggest that Terzan 5 may contain $\sim$11 sources in the range 10^{32-33} ergs s^{-1}, compared to 11 in NGC 6440. A full analysis of the luminosity function and density weighting of quiescent LMXBs in globular clusters will be presented in Heinke et al. (2003, in prep.) We also revise the estimate of the central relaxation time of Terzan 5 to 2×10^8 years from CLG02's value of 4×10^7 years, following Djorgovski's (1993) scaling of $t_{rc} \propto \rho_0^{0.5} r_c^3$. This indicates that the cluster is not as close to the verge of core collapse as suggested by CLG02. The high density of compact binaries in the core seems to be due primarily to the high density of the cluster's massive core. The large numbers of millisecond pulsars (60-200) in the core of Terzan 5 estimated by Fruchter and Goss (2000) would require a long period of high core density to form the millisecond pulsar progenitors. MSPs may be most efficiently formed early in the cluster history by intermediate-mass X-ray binaries (e.g. Davies & Hansen 1998). Therefore it seems likely that Terzan 5's MSPs were formed early in its history, as were those in 47 Tuc (Grindlay et al. 2002), which has a roughly similar inferred ratio ($\sim 15-50$) of MSPs to qLMXBs.

4. CONCLUSIONS

We have presented a reasonable infrared candidate to EXO 1745-248 in Terzan 5, identified by its blue color and positional coincidence with the boresighted *Chandra* position. We have assembled a broad X-ray spectrum using a simultaneous *RXTE* observation and the *Chandra* spectrum from the readout streak, slightly altering the energy scale of the *Chandra* readout spectrum to account for observed gain variation during the readout. We utilized the empirical comparisons of SPO01 to indicate that this LMXB appears similar to other ultracompact LMXBs in globular clusters, suggesting that EXO 1745-248 is the fifth ultracompact LMXB known in a globular cluster. We also identify a broad, strong 6.55 keV iron line, the strongest (EW=188^{+86}_{-83} eV) yet discovered in a globular cluster LMXB, with an accompanying smeared $\sim$ 8.1 keV iron edge.

The superb resolution of *Chandra* has allowed us to identify nine faint X-ray sources within 30" of an LMXB in outburst in Terzan 5. Spectral fitting with bremsstrahlung and power-law models, and a neutron star hydrogen atmosphere model (Lloyd 2003), suggests that four of these sources are qLMXBs, while five are candidate CVs. Artificial point source testing suggests that we are missing $\sim$30% of the sources in the range $L_X(0.5-2.5$ keV) = 10^{32-33} ergs s^{-1} due to the presence of the LMXB in outburst. This implies a total cluster population of $11.4^{+4.7}_{-1.8}(1\sigma)$ sources with $L_X > 10^{32}$ ergs s^{-1} (excluding the LMXB). A recalculation of the central density of Terzan 5 from updated cluster parameters gives log(ρ_0)=5.23, suggesting that Terzan 5 is not the richest of the globular clusters in stellar encounter products and is not as dynamically unstable as previously thought (CLG02). Thus we find that the numbers of X-ray sources in Terzan 5 are consistent with the numbers discovered in other globular clusters and the currently favored formation methods.

Upcoming *Chandra* observations of Terzan 5 and NGC 6440 (PI: R. Wijnands) will allow us to better constrain the variability and spectra of the qLMXBs in those clusters. *V* and *I* observations of Terzan 5, with the *HST* Advanced Camera for Surveys in HRC mode at times when EXO 1745-248 is in outburst vs. quiescence, could unambiguously verify the identification proposed here.

C. H. thanks J. M. Miller, R. Wijnands, T. Gaetz, R. K. Smith, R. Edgar, and the anonymous referee for useful comments that have improved this paper. CH also thanks S. Wachter for access to unpublished data. This work was supported in part by *Chandra* grant GO0-1098A and *HST* grant GO-7889.01-96A. *RXTE* data and results provided by the ASM/*RXTE* teams at MIT and at the *RXTE* SOF and GOF at NASA's GSFC. The Guide Star Catalogue-II is a joint project of the Space Telescope Science Institute and the Osservatorio Astronomico di Torino. This research has made use of the data and resources obtained through the HEASARC on-line service, provided by

NASA-GSFC, the VizieR catalogue access tool, CDS, Strasbourg, France, and NASA's Astrophysics Data System.

REFERENCES

Aldcroft, T. L., Karovska, M., Cresitello-Ditmar, M. L., Cameron, R. A., Markevitch, M. L. 2000, Proc. SPIE, 4012, 650
Arnaud, K. A. 1996, in G. Jacoby & J. Barnes, (eds.) ASP Conf. Series *Astronomical Data Analysis Software and Systems V.*, vol. 101, 17
Asai, K., Dotani, T., Nagase, F., & Mitsuda, K. 2000, ApJS 131, 571
Barret, D., Olive, J. F., Boirin, L., Done, C., Skinner, G. K., & Grindlay, J. E. 2000, ApJ 533, 329
Becker, W. et al. 2003, ApJ submitted (astro-ph/0211468)
Bloser, P. F., Grindlay, J. E., Kaaret, P., Zhang, W., Smale, A. P., & Barret, D. 2000, ApJ 542, 1000
Cohn, H. N., Lugger, P. M., Grindlay, J. E., & Edmonds, P. D. 2002, ApJ 571, 818
Cool, A. M., Haggard, D., Carlin, J. L. 2002, in F. van Leeuwen, J. D. Hughes, G. Piotto (eds.), Omega Centauri, A Unique Window into Astrophysics, Vol. 265 of *ASP Conference Series*, ASP, p. 277
D'Amico, N., Possenti, A., Fici, L., Manchester, R. N., Lyne, A. G., Camilo, F., & Sarkissian, J. 2002, ApJ 570, L89
Daniel, W. W. 1990, *Applied Nonparametric Statistics, 2d ed.*, PWS-Kent
Danner, R., Kulkarni, S. R., Saito, Y., & Kawai, N. 1997, *Nature* 388, 751
Davies, M. B., & Hansen, B. M. S. 1998, MNRAS 301, 15
Deutsch, E. W., Margon, B., & Anderson, S. F. 2000, ApJ, 530, L21
Djorgovski, S. 1993, in S. Djorgovski, G. Meylan (eds.), Structure and Dynamics of Globular Clusters, Vol. 50 of *ASP Conference Series*, ASP, p. 373
Ebisawa, K. et al. 1994, PASJ 46, 375
Edmonds, P. D., Grindlay, J. E., Cohn, H. N., & Lugger, P. M. 2001, ApJ 547, 829
Fruchter, A. S. & Goss, W. M. 2000, ApJ 536, 865
Gehrels, N. 1986, ApJ 303, 336
Giacconi, R. et al. 2001, ApJ 551, 624
Grindlay, J. E., Heinke, C. O., Edmonds, P. D., & Murray, S. S. 2001a, *Science* 292, 2290
Grindlay, J. E., Heinke, C. O., Edmonds, P. D., Murray, S. S., & Cool, A. M. 2001b, ApJ 563, L53
Grindlay, J. E., Camilo, F., Heinke, C. O., Edmonds, P. D., Cohn, H., & Lugger, P. 2002, ApJ in press (available at astro-ph/0208280)
Grindlay, J. E. et al. 2003, AN in press (available at astro-ph/0211527)
Harris, W. E. 1996, AJ, 112, 1487
Heinke, C. O., Edmonds, P. D., Grindlay, J. E. 2001, ApJ 562, 363
Heinke, C. O., Grindlay, J. E., Lloyd, D. A., & Edmonds, P. D. 2002, ApJ, submitted
Hertz, P. & Grindlay, J. E. 1984, ApJ 282, 118
Hünsch, M., Schmitt, J. H. M. M, Sterzik, M. F., & Voges, W. 1999, A&AS, 135, 319
Inoue, H. et al. 1984, PASJ 36, 855
Johnston, H. M., Verbunt, F., & Hasinger, G. 1995, A&A 298, L21
Johnston, H. M. & Verbunt, F. 1996, A&A 312, 80
Jonker, P. G., Mendez, M., Nelemans, G., Wijnands, R., & van der Klis, M 2003, MNRAS (in press; astro-ph/0301475)
Kurucz, R. 1992, Rev.Mex.A.A. 23, 181
Kuulkers, E., den Hartog, P. R., in't Zand, J. J. M., Verbunt, F. W. M., Harris, W. E., & Cocchi, M. 2002, A&A (in press; astro-ph/0212028)
Lloyd, D. A. 2003, MNRAS (submitted)
Lugger, P. M., Cohn, H. N., & Grindlay, J. E. 1996, ApJ 439, 191
Lyne, A. G., Mankelow, S. H., Bell, J. F., & Manchester, R. N. 2000, MNRAS, 316, 491
Makishima, K. et al. 1981, ApJ 247, L23
Makishima, K. et al. 2000, ApJ 535, 632
Markwardt, C. B. & Swank, J. H. 2000a, IAU Circ. 7454
Markwardt, C. B., Strohmayer, T. E., Swank, J. H., & Zhang, W. 2000b, IAU Circ. 7482
Merloni, A., Fabian, A. C., & Ross, R. R. 2000, MNRAS 313, 193
Ortolani, S., Barbuy, B., & Bica, E. 1996, A&A 308, 733
Ortolani, S., Barbuy, B., Bica, E., Renzini, A., Zoccali, M., Rich, R. M., & Cassisi, S., A&A, 2001, 376, 878
Parmar, A. N., Oosterbroek, T., Sidoli, L, Stella, L., & Frontera, F. 2001, A&A 380, 490
Pooley, D., et al. 2002, ApJ 569, 405
Pooley, D., et al. 2002, ApJ 573, 184
Predehl, P. & Schmitt, J. H. M. M. 1995, A&A 293, 889
Rutledge, R. E., Bildsten, L., Brown, E. F., Pavlov, G. G., & Zavlin, V. E. 2001c, ApJ 578, 405
Shimura, T., & Takahara, F. 1995, ApJ 445, 780
Sidoli, L, Parmar, A. N., Oosterbroek, T., Stella, L., Verbunt, F., Masetti, N., & Dal Fiume, D. 2001, A&A 368, 451
Smale, A. P. 1995 AJ, 110, 1292
Smith, R. K., Edgar, R. J., & Shafer, R. A. 2002, ApJ 581, 562
Titarchuk, L. 1994, ApJ 434, 570
Trager, S. C., King, I. R., & Djorgovski, S. 1995, AJ, 109, 218
van Paradijs, J. & McClintock, J. E. 1994, A&A, 290, 133
van Paradijs, J. & McClintock, J. E. 1995, in X-ray Binaries, ed. Lewin, van Paradijs, van den Heuvel (Cambridge U. Press), p. 58
Verbunt, F., & Hut, P. 1987, IAU Symp. 125, 187
Verbunt, F., Bunk, W., Hasinger, G. & Johnston, H. M., 1995, A&A, 300, 732
Verbunt, F. 2002, in ASP Conf. Ser. *ω Centauri, a unique window in astrophysics*, ed. van Leeuwen, Piotto, Hughes (available at astro-ph/0111441)
Wachter, S. 1997, ApJ 485, 839
Wachter, S. 1998, Ph.D. thesis, University of Washington
Wang, Z. et al. 2001, ApJ 563, L61

TABLE 1
NAMES, POSITIONS AND COUNTS OF DETECTED SOURCES

Source Name (Label)	RA (17:)	Dec (-24:)	0.5-4.5 keV (counts)	0.5-1.5 keV (counts)	1.5-6 keV (counts)
EXO 1745-248 (LMXB)	48:05.196±.015	46:47.40±.20	-	-	-
CXOGLB J174806.1-244642.9 (W2)	48:06.154±.005	46:42.68±.07	37±10	11±4	20±10
CXOGLB J174805.3-244637.7 (W3)	48:05.370±.004	46:37.66±.05	77±13	30±6	41±13
CXOGLB J174804.7-244644.6 (W4)	48:04.799±.003	46:44.64±.06	17±19	15±7	-1±21
CXOGLB J174804.4-244638.2 (W5)	48:04.402±.006	46:38.15±.09	81±11	13±4	80±12
CXOGLB J174804.3-244703.8 (W6)	48:04.366±.004	47:03.75±.07	180±16	22±5	208±17
CXOGLB J174804.2-244641.8 (W7)	48:04.214±.005	46:41.79±.09	85±11	10±4	86±12
CXOGLB J174804.2-244648.4 (W8)	48:04.225±.05	46:48.34±.2	34±12	15±5	30±12
CXOGLB J174804.0-244640.5 (W9)	48:04.059±.009	46:40.53±.06	50±10	4±3	53±11
CXOGLB J174803.5-244649.2 (W10)	48:03.539±.005	46:49.24±.08	69±11	8±4	75±12
Sources not associated with Terzan 5					
CXOU J174803.3-244854.1 (Star 1)	48:03.334±.004	48:54.04±.06	45±8	36±7	9±5
CXOU J174751.7-244657.4	47:51.726±.010	46:57.42±.11	36±7	9±4	35±7
CXOU J174814.7-244802.2	48:14.703±.011	48:02.21±.12	29±7	7±4	28±6
CXOU J174812.6-244811.1 (Star 2)	48:12.649±.010	48:11.10±.13	28±8	20±6	6±5

Note. — Sources detected in and around Terzan 5. RA and Declination values for cluster members begin with 17: and -24:, respectively. Errors are centroiding errors within the (shifted to match GSC 2.2) *Chandra* frame, and do not include systematic errors incurred in matching to other frames (absolute errors perhaps 0.″5; see text). Counts in each energy band were determined by subtracting the average count rate in surrounding 2" annulus from the counts in 1" circle around source position (leading to one negative entry).

TABLE 2
SPECTRAL FITS TO FAINT SOURCES

Source	H-atmosphere		Bremsstrahlung		Powerlaw		0.5-2.5 L_X
	(kT, eV)	(χ^2_ν/dof)	(kT, keV)	(χ^2_ν/dof)	(α)	(χ^2_ν/dof)	(ergs s^{-1})
W2	98^{+5}_{-6}	1.19/14	$0.7^{+0.5}_{-0.3}$	1.16/13	$3.9^{+1.1}_{-1.0}$	1.31/13	4.1×10^{32}
W3	104^{+5}_{-5}	1.36/22	$1.0^{+0.7}_{-0.3}$	1.05/21	$3.1^{+0.8}_{-0.6}$	1.20/21	5.6×10^{32}
W4	90^{+9}_{-17}	1.37/11	$0.5^{+2.5}_{-0.5}$	1.49/10	$4.6^{+\infty}_{-2.6}$	1.5/10	2.7×10^{32}
W5	92	3.0/16	$6.3^{+71}_{-3.8}$	1.29/15	$1.7^{+0.5}_{-0.5}$	1.34/15	1.9×10^{32}
W6	100	4.42/33	>29	1.08/32	$1.0^{+0.3}_{-0.2}$	1.05/32	3.5×10^{32}
W7	90	2.50/16	>6	0.51/15	$1.2^{+0.5}_{-0.5}$	0.51/15	1.5×10^{32}
W8	92^{+6}_{-9}	0.84/19	$0.8^{+1.7}_{-0.4}$	0.78/18	$3.3^{+1.8}_{-1.3}$	0.82/18	3.1×10^{32}
W9	79	2.27/13	>2	1.37/12	$1.3^{+0.9}_{-0.8}$	1.37/12	8.6×10^{31}
W10	88	2.92/15	>7	0.95/14	$1.1^{+0.6}_{-0.6}$	0.94/14	1.3×10^{32}

Note. — Spectral fits to faint cluster sources, with background subtraction, in XSPEC. All fits include photoelectric absorption fixed at the cluster N_H, 1.2×10^{22} cm^{-2}. Hydrogen atmosphere fits are made with radius fixed to 10 km. X-ray luminosities are unabsorbed for the range 0.5 to 2.5 keV, from hydrogen-atmosphere NS fits (W2, W3, W4, W8) or thermal bremsstrahlung fits. Errors in all the tables are 90% confidence for a single parameter.

TABLE 3
SPECTRAL FITS TO LMXB EXO 1745-248 CONTINUUM

Model	N_H	COMPTT			BB or DiskBB[a]			χ^2_ν/dof
	(10^{22} cm^{-2})	(kT$_0$)	(kT$_e$)	(τ_p)	(kT)	(R, km)	(f[b])	
DBB	$1.72^{+.20}_{-.17}$	$1.29^{+.40}_{-.13}$	$10.2^{+.5}_{-.4}$	$8.1^{+.3}_{-.4}$	$0.80^{+.38}_{-.16}$	$8.7^{+5.0}_{-4.4}$	0.12	1.06/225
BB	$1.46^{+.19}_{-.17}$	$1.21^{+.24}_{-.09}$	$10.2^{+.5}_{-.4}$	$8.1^{+.3}_{-.2}$	$0.53^{+.05}_{-.06}$	$20.6^{+6.2}_{-5.1}$	0.07	1.06/225

Note. — Spectral fits to the LMXB EXO 1745-248 from *RXTE* data and the *Chandra* readout streak with energy scale alteration (see text), with background subtraction in XSPEC. A gaussian, a smeared edge, photoelectric absorption, and comptonization using the XSPEC model COMPTT is included in both fits. The first also includes a multicolor disk-blackbody (DBB), while the second includes a blackbody (BB). Values are in keV unless otherwise noted (f and τ_p are unitless). Values from normalizations utilize the PCA normalizations; uncertainty in PCA absolute normalization is not included.

[a]kT and R refer to the inner edge of the diskbb for model 1 (where R is $R_{in}\cos(i)^{0.5}$), and to the blackbody for model 2.

[b]f is the ratio of the blackbody or diskbb flux to COMPTT flux, over 0.1-100 keV range.

TABLE 4
SPECTRAL FITS TO LMXB EXO 1745-248 FEATURES

Gaussian	
kT	$6.55^{+.06}_{-.07}$
EW (eV)	188^{+86}_{-83}
σ	$0.31^{+.16}_{-.15}$
Smeared edge	
kT	8.1 ± 0.8
$\tau_{\max}$	$0.25^{+1.22}_{-.16}$
Width	$2.6^{+5.5}_{-2.0}$

Note. — Spectral fits to the Fe-line gaussian and disk reflection smeared edge in the spectrum of the LMXB EXO 1745-248. The spectral fits in this table are to the "standard model" including a multi-color disk-blackbody (see text); line and edge parameter values for the other model considered in the text are within the errors in this table. Values are in keV unless otherwise stated, except $\tau_{\max}$ which is unitless.

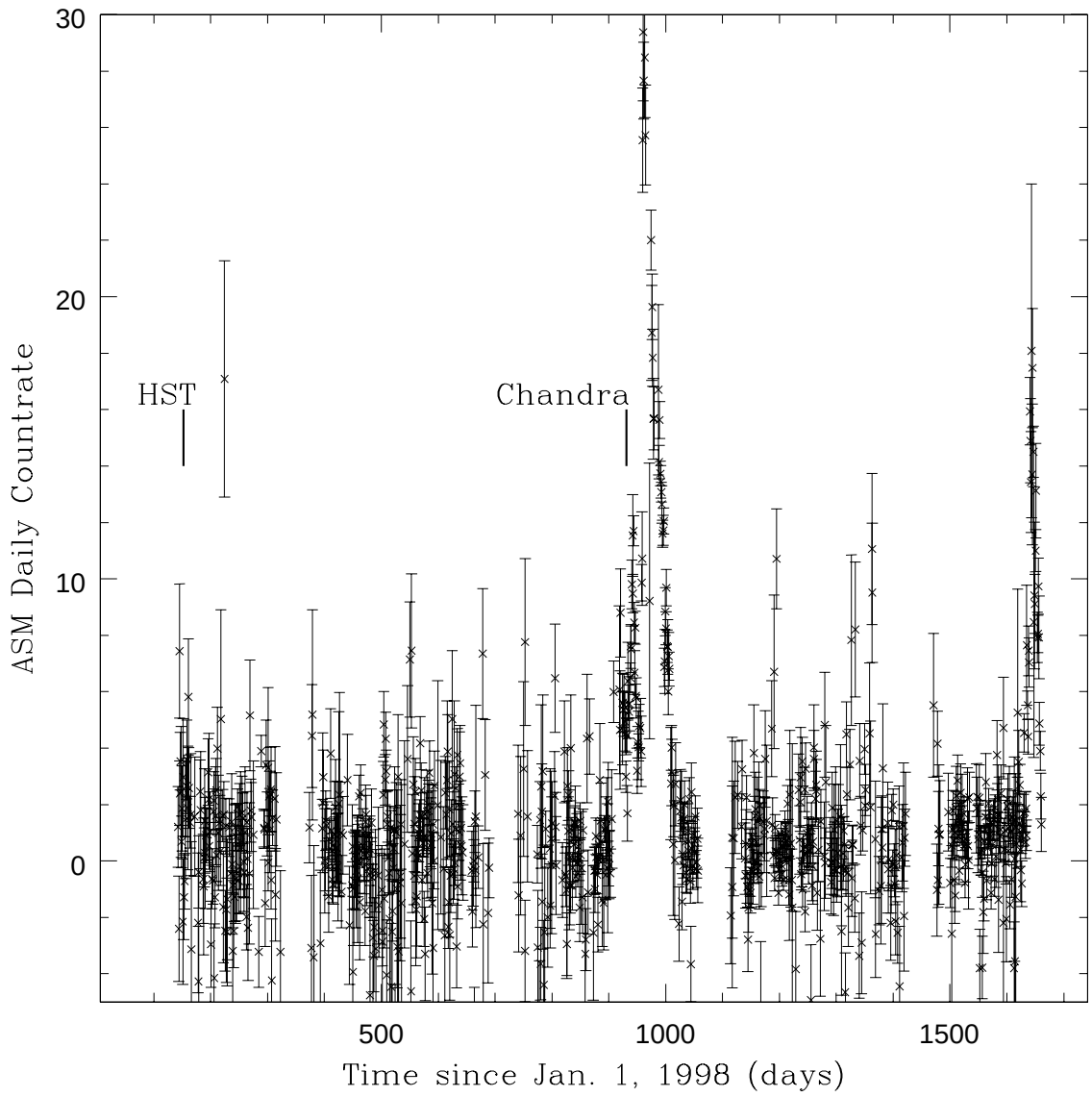

FIG. 1.— The *RXTE* All-Sky Monitor lightcurve of the LMXB EXO1748-25 in Terzan 5. The dates of the *Chandra* and *HST* observations are marked.

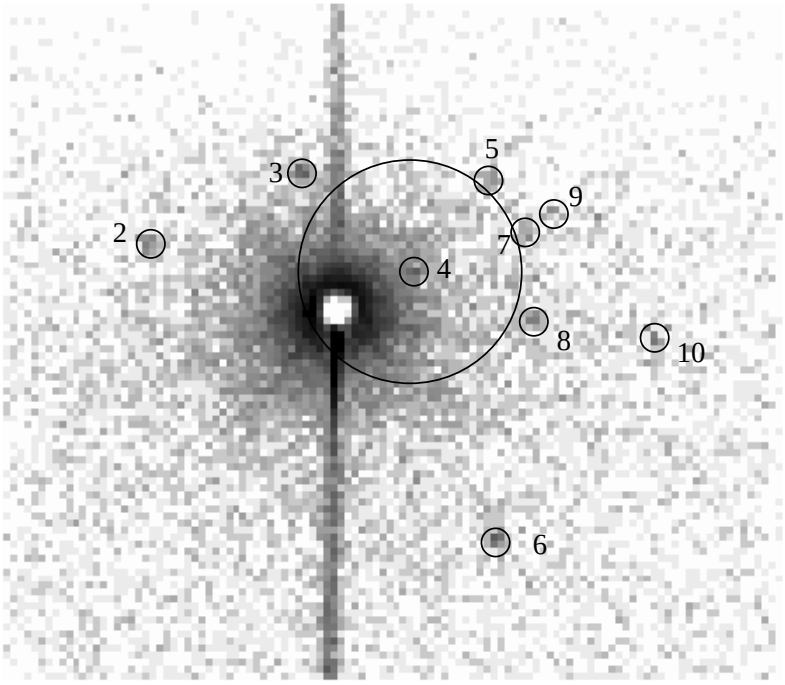

FIG. 2.— *Chandra* ACIS-I image of the globular cluster Terzan 5, energy range 0.5-2.0 keV. The dominant feature is the piled-up halo from the LMXB EXO 1745-248 in its high state. The streak is due to out-of-time LMXB events recorded during the frame transfer, and the position of the LMXB has no good events due to pulse saturation. Several other sources are visible, marked with 1" circles and indicated with their shorthand names. The cluster core is indicated with a 7.9" (1 r_c) circle.

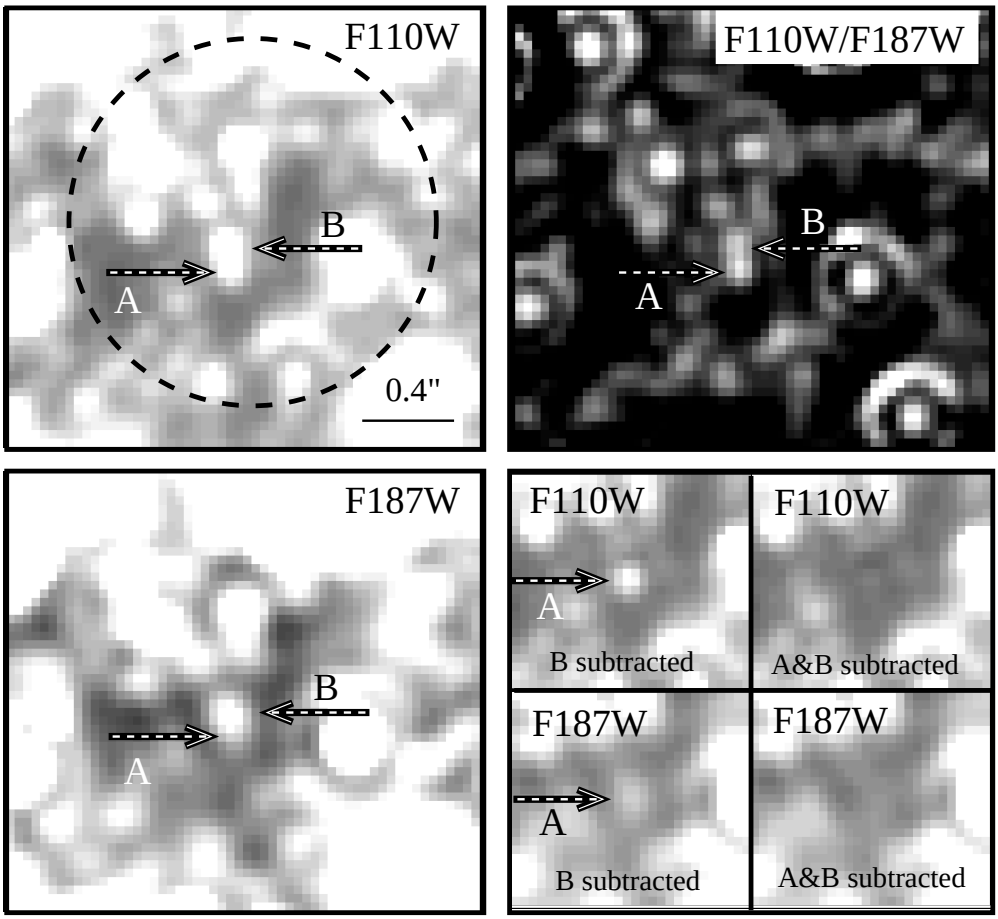

FIG. 3.— Finding chart, showing stars A and B in F110W (upper left) and F187W (lower left) *HST* NICMOS data, and the ratio image F110W/F187W (upper right). The best estimate of the uncertainty in the position of EXO 1745-248 is indicated by the 0.8" (2 σ) error circle. Note that star A is the bluest object in this field (some red giant cores appear blue due to saturation). The results of our manual psf fitting of stars A and B are shown at lower right.

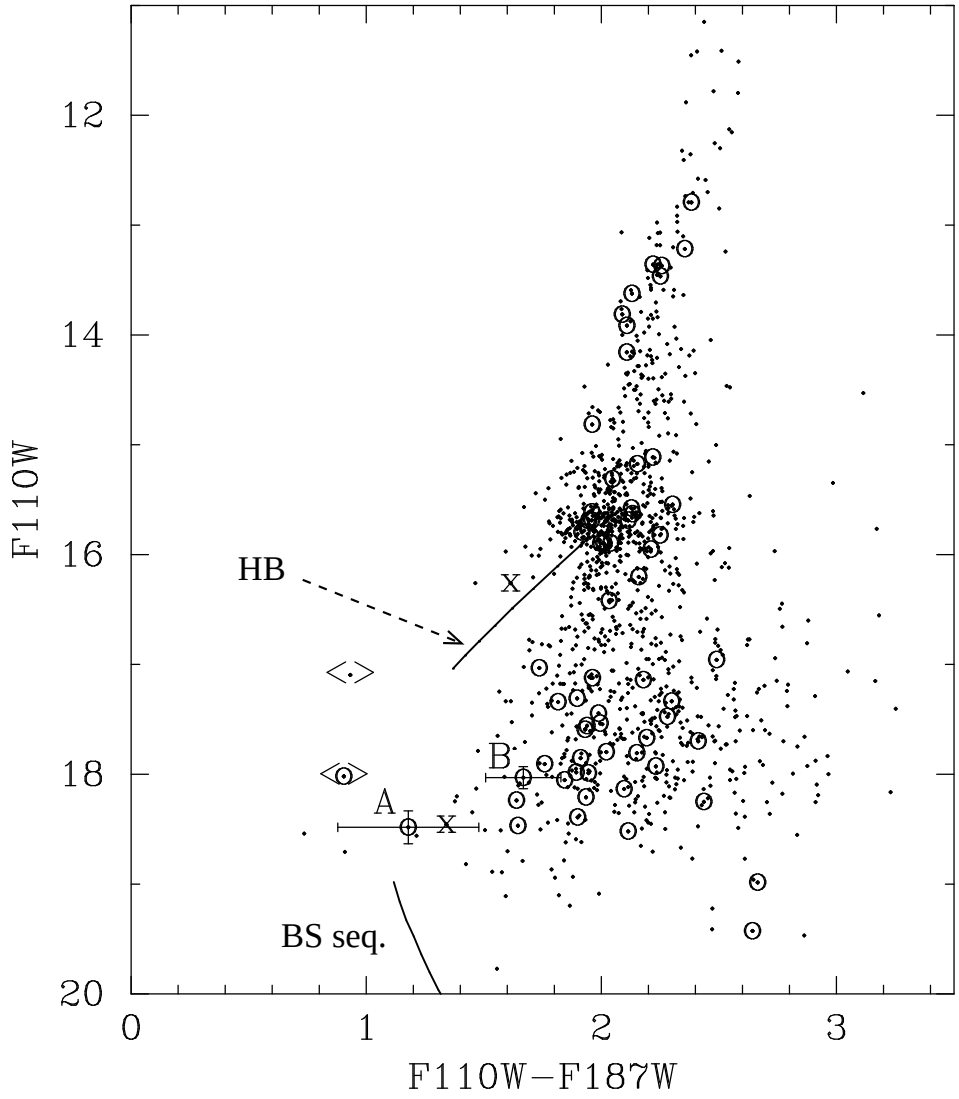

FIG. 4.— Aperture photometry color-magnitude diagram of Terzan 5, from the *HST* NIC2 camera (using highly dithered imaging via the drizzle algorithm) on the core of Terzan 5. Stars from the photometry of EGC01 within 1" of the seven X-ray error circles are circled. Xs mark the locations of variable stars from EGC01 (X2 is the dimmer one). Two stars that are more than 3 σ to the blue of the distribution are indicated by $< . >$. The lower is the blend of stars A and B (see text). The separately derived positions of stars A and B are indicated, with errors from the photometry. The horizontal branch and the expected blue straggler sequence, terminating in a Kurucz model (Kurucz 1992) of a 1.6 $M_{\odot}$ star (twice the turnoff mass) are indicated.

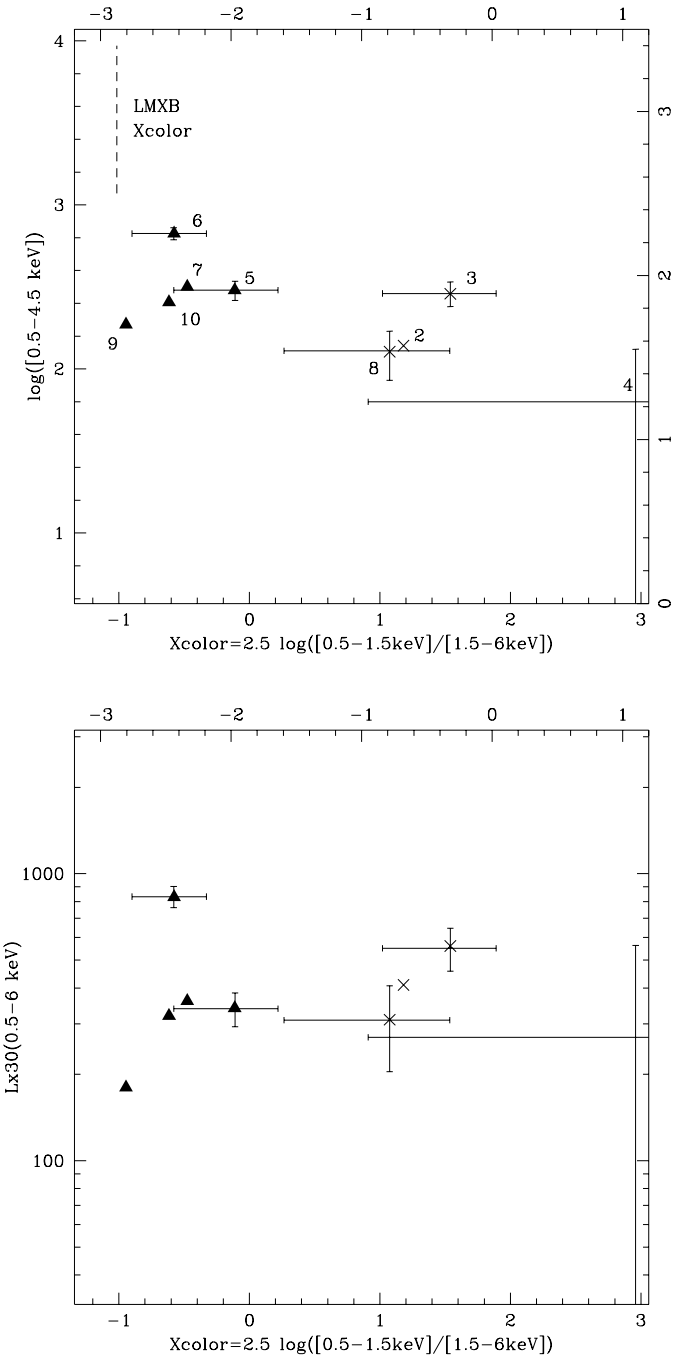

FIG. 5.— X-ray color-magnitude diagrams of Terzan 5. Upper panel produced from the absorption-corrected counts in the 0.5-1.5, 0.5-4.5, and 1.5-6 keV energy bands (lower and left axes; upper and right axes provide the observed colors and magnitudes). We correct roughly for photoelectric absorption by shifting the data +0.57 units on the left axis and +1.86 units on the bottom axis. However, note that the effects of absorption are not uniform. The probable qLMXBs are marked by crosses, and probable CVs by filled triangles. We plot representative errors for a few points. Background subtraction leaves W4 with -1 counts in the hard band; we show its Xcolor lower limit and counts range (it is only clearly detected in the soft band). The Xcolor of EXO 1745-248's X-ray halo is indicated with a dotted line and labeled 'LMXB Xcolor'. Lower panel produced using the same absorption-corrected color for x axis, but using the unabsorbed 0.5-6 keV luminosity for y axis. Luminosities derived from best-fitting hydrogen atmosphere fits for W2, W3, W4, and W8, and best-fitting thermal bremsstrahlung fit for W5, W6, W7, W9, and W10. Luminosity errors are based on 0.5-4.5 keV counting statistics, and do not include uncertainties in spectral fitting.

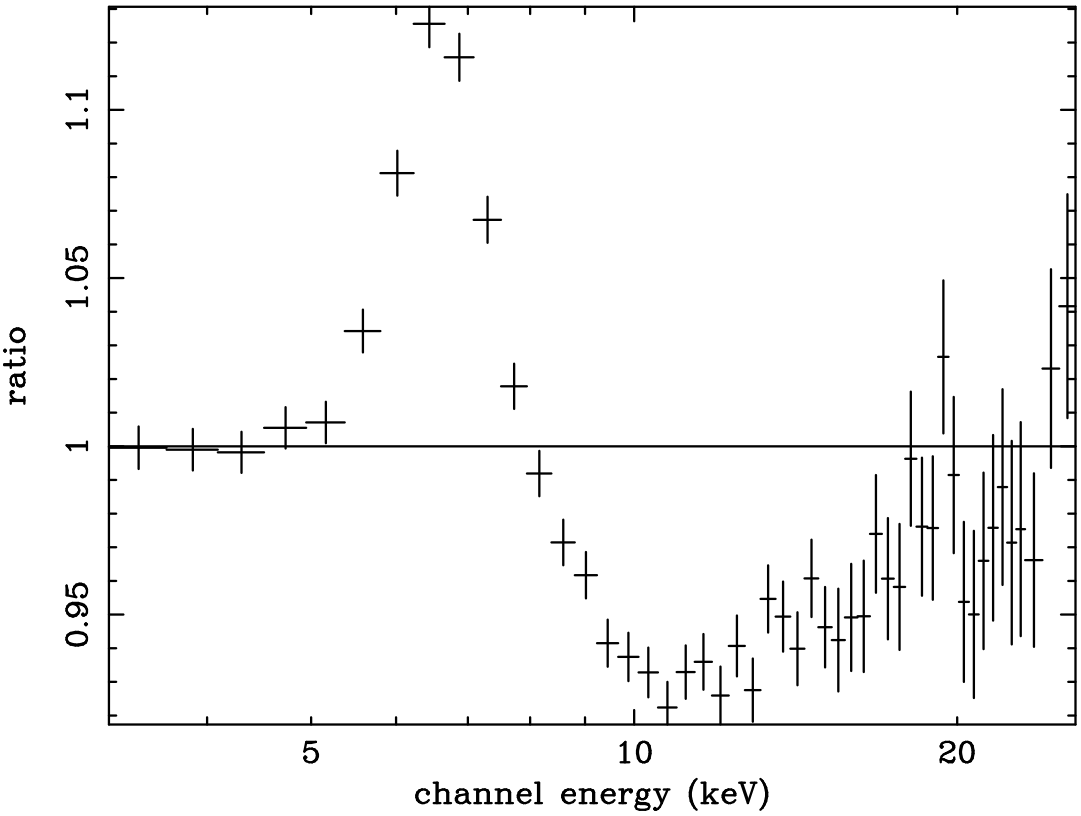

FIG. 6.— Ratio of EXO 1745-248 PCA data to standard model (see text), with normalizations of the gaussian iron line and smeared edge set to zero to show the relative contributions.

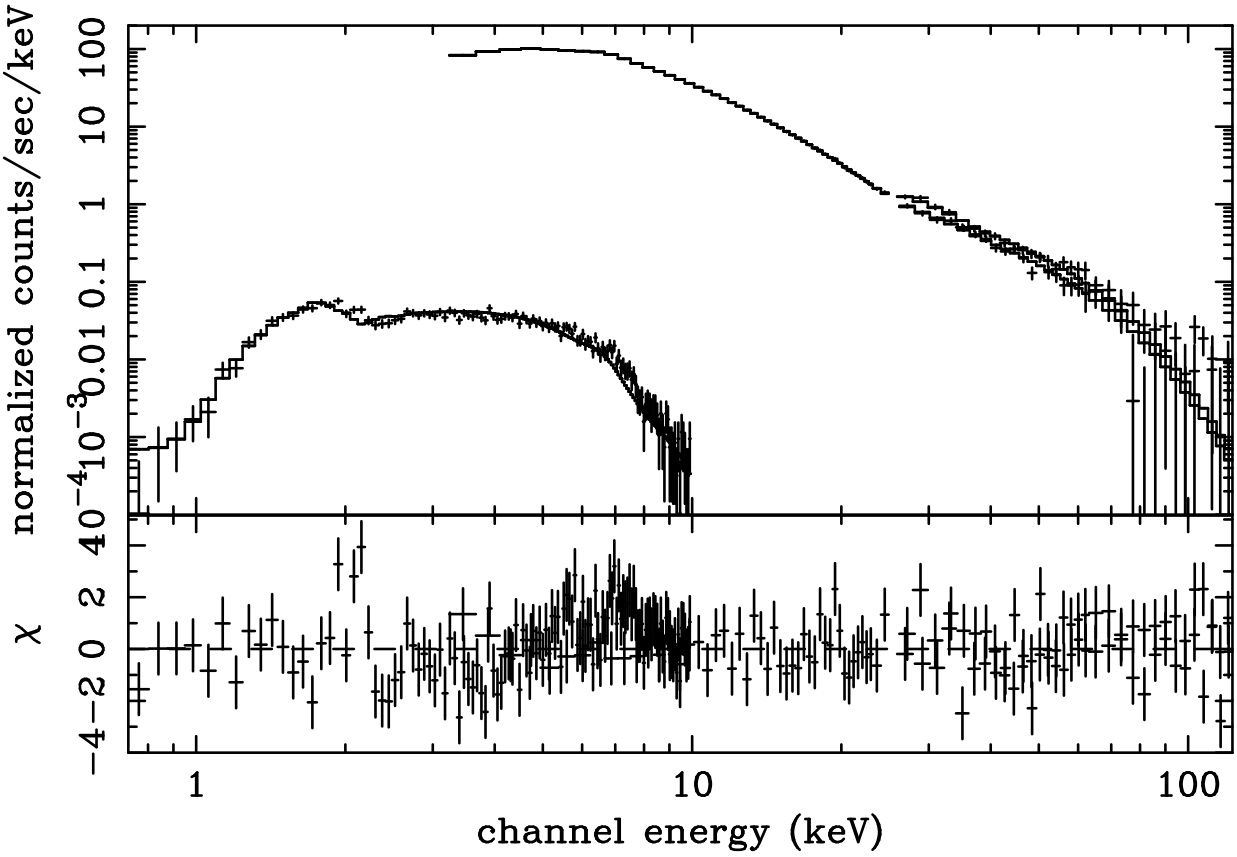

FIG. 7.— EXO 1745-248 spectrum from *Chandra* readout streak data, *RXTE* PCA, and *RXTE* HEXTE data, simultaneously fitted with the standard model (see text). Note the poor fit to the *Chandra* data near 2 keV and the pronounced wave above 5 keV, suggesting an incorrect energy calibration.

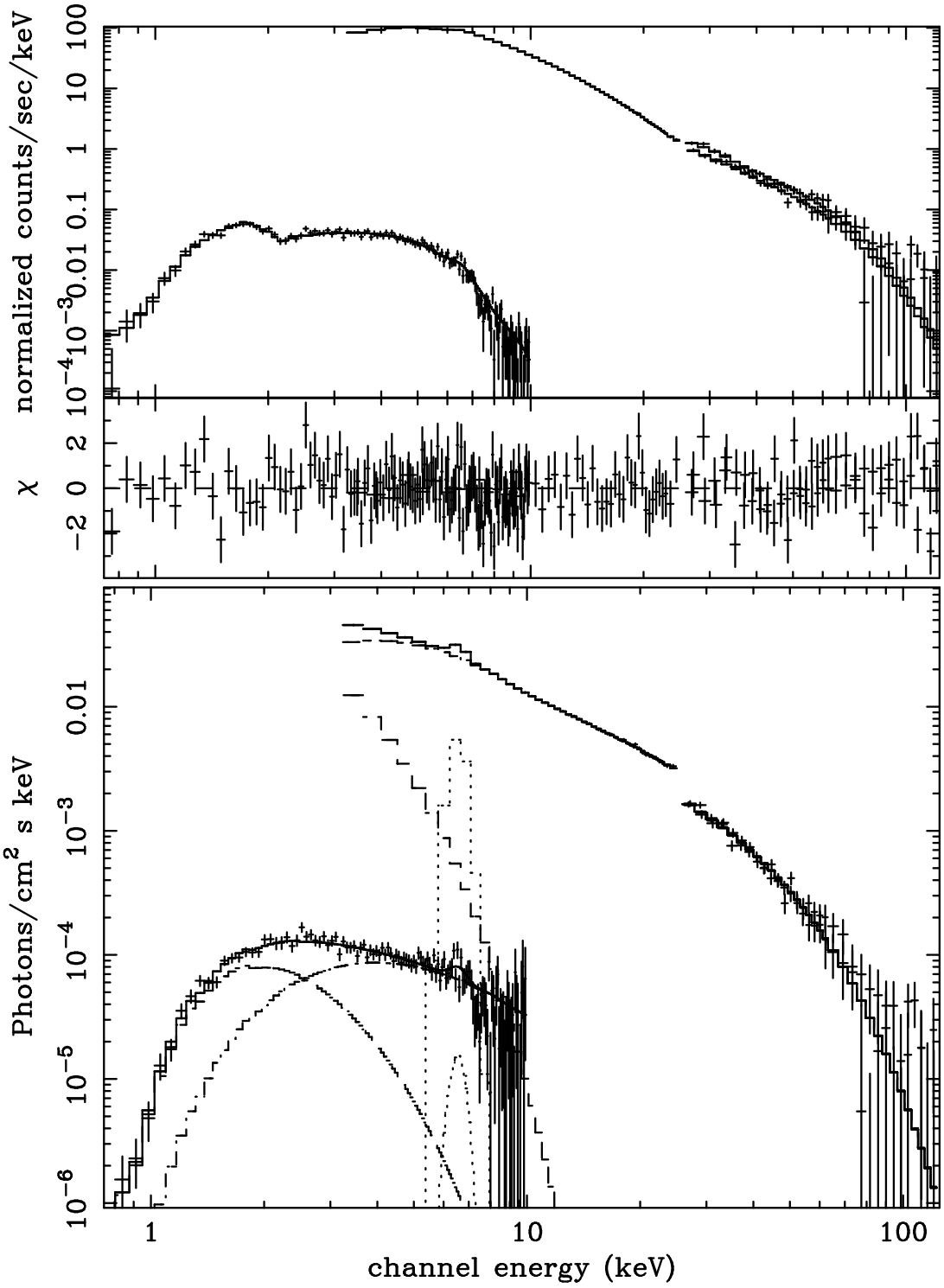

FIG. 8.— EXO 1745-248 observed (top) and unfolded (bottom) spectra, with best-fit absorbed (DISKBB+COMPTT+GAUSSIAN)×SMEDGE model spectrum. Here the energies assigned to *Chandra* readout streak events have been increased by 7%. Relative normalizations of the different instruments are allowed to vary (see text). The 6.55 keV iron line is visible in both the *RXTE* and *Chandra* unfolded spectra, along with the DISKBB and COMPTT components (the COMPTT is the harder component).